



# Incorporating Si<sub>3</sub>N<sub>4</sub> into PEEK to Produce Antibacterial, Osteoconductive, and Radiolucent Spinal Implants

Giuseppe Pezzotti,\* Elia Marin, Tetsuya Adachi, Federica Lerussi, Alfredo Rondinella, Francesco Boschetto, Wenliang Zhu, Takashi Kitajima, Kosuke Inada, Bryan J. McEntire, Ryan M. Bock, B. Sonny Bal, and Osam Mazda

Polyetheretherketone (PEEK) is a popular polymeric biomaterial which is primarily used as an intervertebral spacer in spinal fusion surgery; but it is developed for trauma, prosthodontics, maxillofacial, and cranial implants. It has the purported advantages of an elastic modulus which is similar to native bone and it can be easily formed into custom 3D shapes. Nevertheless, PEEK's disadvantages include its poor antibacterial resistance, lack of bioactivity, and radiographic transparency. This study presents a simple approach to correcting these three shortcomings while preserving the base polymer's biocompatibility, chemical stability, and elastic modulus. The proposed strategy consists of preparing a PEEK composite by dispersing a minor fraction (i.e., 15 vol%) of a silicon nitride (Si<sub>3</sub>N<sub>4</sub>) powder within its matrix. In vitro tests of PEEK composites with three Si<sub>3</sub>N<sub>4</sub> variants— $\beta$ -Si<sub>3</sub>N<sub>4</sub>,  $\alpha$ -Si<sub>3</sub>N<sub>4</sub>, and  $\beta$ -SiYAlON—demonstrate significant improvements in the polymer's osteoconductive versus SaOS-2 cells and bacteriostatic properties versus gram-positive *Staphylococcus epidermidis* bacteria. These properties are clearly a consequence of adding the bioceramic dispersoids, according to chemistry similar to that previously demonstrated for bulk Si<sub>3</sub>N<sub>4</sub> ceramics in terms of osteogenic behavior (vs both osteosarcoma and mesenchymal progenitor cells) and antibacterial properties (vs both gram-positive and gram-negative bacteria).

## 1. Introduction

Polyetheretherketone (PEEK) is a semi-crystalline aromatic polymer which belongs to the polyaryletherketone family. Its molecular backbone includes combinations of ketone and ether functional groups between the aryl rings.<sup>[1]</sup> This peculiar structure makes it chemically stable in biologically active environments.<sup>[1–3]</sup> It also provides the polymer with improved wear resistance<sup>[2,4]</sup> and the retention of mechanical properties under either steam or gamma sterilization.<sup>[5]</sup> PEEK is bioinert and biocompatible. It elicits no toxic, mutagenic, or inflammatory responses within the human body.<sup>[6–9]</sup> Moreover, its elastic modulus is close to that of human cortical bone (8.3 and 17.7 GPa, respectively),<sup>[10]</sup> a characteristic which has been widely exploited in spinal implants to minimize stress shielding and bone resorption.<sup>[11]</sup> However, the biological inertness of PEEK comes with

G. Pezzotti, F. Lerussi, A. Rondinella, F. Boschetto, W. Zhu, E. Marin  
Ceramic Physics Laboratory  
Kyoto Institute of Technology  
Sakyo-ku, Matsugasaki, 606-8585 Kyoto, Japan  
E-mail: pezzotti@kit.ac.jp

G. Pezzotti  
Department of Orthopedic Surgery  
Tokyo Medical University  
6-7-1 Nishi-Shinjuku  
Shinjuku-ku, 160-0023 Tokyo, Japan

G. Pezzotti  
The Center for Advanced Medical Engineering and Informatics  
Osaka University  
Yamadaoka  
Suita, 565-0871 Osaka, Japan

G. Pezzotti  
Department of Immunology  
Graduate School of Medical Science  
Kyoto Prefectural University of Medicine Kamigyo-ku  
465 Kajii-cho  
Kawaramachi dori, 602-0841 Kyoto, Japan

DOI: 10.1002/mabi.201800033

E. Marin, T. Adachi  
Department of Dental Medicine  
Graduate School of Medical Science  
Kyoto Prefectural University of Medicine  
Kamigyo-ku, Kyoto 602-8566, Japan

F. Lerussi  
Department of Molecular Sciences and Nanosystems  
Ca' Foscari University of Venice  
Dorsoduro 2137, 30123 Venezia, Italy

F. Boschetto, O. Mazda  
Department of Immunology  
Kyoto Prefectural University of Medicine  
Kamigyo-ku, Kyoto 602-8566, Japan

T. Kitajima  
Functional Composite Material Laboratory  
Otsuka Chemical Co., Ltd.  
2-2 Tsukasa-cho  
Chiyoda-ku, 101-0048 Tokyo, Japan

K. Inada  
Market and Research Department  
Otsuka Chemical Co., Ltd.  
2-2 Tsukasa-cho  
Chiyoda-ku, 101-0048 Tokyo, Japan

several disadvantages. It has low bioactivity and it is prone to bacterial colonization, biofilm formation, and periprosthetic infections.<sup>[12–15]</sup> These shortcomings are an unfortunate consequence of a combination of its hydrophobic character and specific molecular interactions between the bacterial proteins and PEEK's surface molecular structure in the biological environment.<sup>[16]</sup> Consequently, functionalization of PEEK to concurrently boost its osteogenic and antibacterial properties is actively being pursued in order to develop an improved generation of trauma, spinal, prosthodontic, maxillofacial, and cranial implants.<sup>[17–19]</sup> The two strategies currently used to improve the bioactivity and the antimicrobial properties of PEEK are surface functionalization and composites.

Surface functionalization has been accomplished by changing PEEK's surface chemistry and topology using either chemical or physical alterations (e.g., coatings, infiltration of chemicals, mechanical roughening, polishing, and texturing).<sup>[20]</sup> PEEK composites have been prepared by incorporating nanometer or micrometer particles that provide PEEK with osteoconductive and antibacterial characteristics.<sup>[21,22]</sup> Unfortunately, none of these approaches have succeeded in concurrently achieving both biogenic and bactericidal properties. Antiadhesive surfaces, such as hydrophobic coatings, have been proposed as a method of preventing periprosthetic infections. While these coatings resist the adherence of prokaryotic cells,<sup>[22–27]</sup> they also result in poor protein and eukaryotic cell adhesion which ultimately leads to a lack of tissue integration.<sup>[22]</sup> Although the direct incorporation of antiseptics and antibiotics into the polymer's structure has been demonstrated, controlling their elution kinetics<sup>[24]</sup> has proven to be particularly challenging and especially inoperative against antibiotic-resistant bacterial strains.<sup>[28]</sup> Moreover, this approach is not effective in improving the osteointegration of these types of devices. Last, plasma gas treatments of PEEK surfaces have been shown to produce only temporary osseointegrative benefits.<sup>[29]</sup>

Regarding the composite approach, the most popular fillers to polymeric matrices have been hydroxyapatite (HAp) and silver particles for improving biogenesis<sup>[30]</sup> and antibacterial<sup>[31]</sup> properties, respectively. Zhang et al. manufactured PEEK-matrix hydroxyapatite composites via selective laser sintering and evaluated in vitro cell attachment, morphology, proliferation, and differentiation of primary human osteoblasts.<sup>[32]</sup> These composites supported osteoblast growth and enhanced cell proliferation and osteogenic differentiation compared to other polymeric biomaterials. Silver particles have proven to be suitable antibacterial agents against a wide range of both gram-positive and gram-negative bacteria.<sup>[33]</sup> Silver is used in dental resin composites<sup>[34,35]</sup> and as an antimicrobial coating on catheters.<sup>[36]</sup> It has shown relatively low cellular toxicity when compared to other metals.<sup>[37]</sup> Nevertheless, currently there

are no PEEK-Ag composites that can simultaneously provide osteogenic and bacteriostatic improvements. Furthermore, development of these types of implantable devices could be an insuperable objective.

In this study, a composite approach was undertaken with the objective of fabricating a material that could concurrently provide high resistance to bacterial colonization and improved osseointegration. With this twofold purpose in mind, a minor fraction of Si<sub>3</sub>N<sub>4</sub> particles was incorporated into a PEEK matrix. Si<sub>3</sub>N<sub>4</sub> was selected because the surface chemistry of this nonoxide bioceramic has previously demonstrated both bacterial lysis<sup>[13,38]</sup> and enhanced bone formation.<sup>[39–41]</sup> These properties resulted from its biologically friendly silicon/nitrogen surface chemistry and its slow elution rate which was suitable for implant applications. In this study, this peculiar chemistry was incorporated into a PEEK polymer for the first time. In this in vitro study, three Si<sub>3</sub>N<sub>4</sub> phases—β-Si<sub>3</sub>N<sub>4</sub>, α-Si<sub>3</sub>N<sub>4</sub>, and β-SiYAlON—were evaluated to compare their osteogenic and bacteriostatic responses when admixed with polyetheretherketone.

## 2. Experimental Section

### 2.1. Material Fabrication

PEEK powder with an average particle size of 25 μm (Victrex PEEK 450G, Victrex PLC, Thornton Cleveleys, Lancashire, UK) was admixed with 15 vol% of three different Si<sub>3</sub>N<sub>4</sub> powders to form three separate PEEK composite batches. The three Si<sub>3</sub>N<sub>4</sub> powders were: i) β-Si<sub>3</sub>N<sub>4</sub> with an average particle size ≈1 μm (MC<sup>2</sup>Si<sub>3</sub>N<sub>4</sub>, Amedica Corporation, Salt Lake City, USA); ii) a submicrometer α-Si<sub>3</sub>N<sub>4</sub> powder (SN-E10, Ube Industries, Ube City, Japan); and iii) a β-SiYAlON powder prepared by Amedica Corporation from a mixture of Si<sub>3</sub>N<sub>4</sub>, Al<sub>2</sub>O<sub>3</sub>, and Y<sub>2</sub>O<sub>3</sub> blended and reacted in N<sub>2</sub> gas atmosphere at >1600 °C for 2 h to obtain N/Si, O/Si, and Y/Si atomic ratios equal to 1.02, 0.50, and 0.064, respectively. The powder was subsequently comminuted to achieve a particle size of ≈1 μm.

The three composites were prepared separately by mixing the PEEK and Si<sub>3</sub>N<sub>4</sub> powders by means of a twin-screw kneader (LABO PLASTOMILL 4C150; Toyo Seiki Seisaku-Sho, Ltd., Tokyo, Japan) while simultaneously heating them to 380 °C. PEEK melts at a temperature which leaves the ceramic particles completely unaltered (i.e., glass transition and melting temperatures are ≈143 and 343 °C, respectively). It was therefore possible to prepare dense PEEK/ceramic composites at a temperature above the melting temperature of the PEEK matrix while fully retaining the chemistry of the particulate fillers. Unfilled (i.e., monolithic) PEEK was also prepared under exactly the same conditions and used as a negative control within the experiments. Optical photos of the composites and enlarged images of their surfaces are shown in **Figure 1a–d** for monolithic PEEK, PEEK/β-Si<sub>3</sub>N<sub>4</sub>, PEEK/α-Si<sub>3</sub>N<sub>4</sub>, and PEEK/β-SiYAlON, respectively. All samples were investigated after manually polishing their surfaces on diamond paper in order to achieve comparable roughness values. This procedure was selected to eliminate differences due to different topographic characteristics of the surfaces, which were

B. J. McEntire, R. M. Bock, B. S. Bal  
Amedica Corporation  
1885 West 2100 South  
Salt Lake City, UT 84119, USA  
B. S. Bal  
Department of Orthopaedic Surgery  
University of Missouri  
Columbia, MO 65212, USA

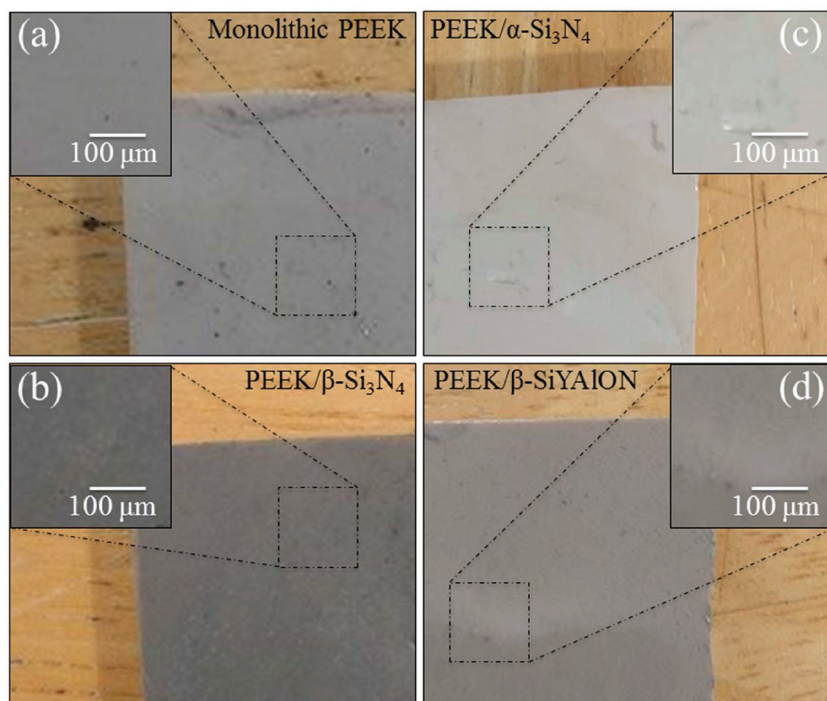


**Figure 1.** Optical photographs of the composite plates and their enlarged microscopic images in the inset: a) monolithic PEEK, b) PEEK/ $\beta$ - $\text{Si}_3\text{N}_4$ , c) PEEK/ $\alpha$ - $\text{Si}_3\text{N}_4$ , and d) PEEK/ $\beta$ -SiAlON.

considered to be only a secondary effect as compared to surface chemistry, and thus to single out the chemical effect arising from adding the ceramic particulate dispersion. All test samples were UV sterilized prior to biological testing.

## 2.2. Bacterial Culture and Characterization

Gram-positive *Staphylococcus epidermidis* (*S. epidermidis*; 14990ATCC) was cultured at the Kyoto Prefectural University of Medicine in a brain heart infusion (BHI) agar culture medium. The initial concentration of  $1.8 \times 10^{10}$  CFU  $\text{mL}^{-1}$  was subsequently diluted to  $1 \times 10^8$  CFU  $\text{mL}^{-1}$  using a phosphate-buffered saline solution (PBS) to mimic ion blood concentrations. Subsequently, 100  $\mu\text{L}$  aliquots of the bacteria solution were transferred to Petri dishes containing the BHI agar and composite samples. Incubation occurred at 37 °C under aerobic conditions for 24 h followed by biological testing.

Bacterial samples were observed using a fluorescence microscopy (BZ-X700; Keyence, Osaka, Japan). Prior to microscopy examination, the bacteria were stained with 5(6)-carboxyfluorescein diacetate (CFDA) and 4',6-diamidino-2-phenylindole (DAPI). CFDA stained the living bacteria with a green color, while DAPI, which binds to DNA, verified cell nuclei locations via a blue stain. The metabolic activity of the bacteria was observed using a colorimetric assay (Microbial Viability Assay Kit-WST, Dojindo, Kumamoto, Japan). This assay employed an indicator (WST-8), which produced a water-soluble formazan dye upon reduction in the presence of an electron mediator. The amount of the formazan dye generated was directly proportional to the number of living microorganism. Solutions were

analyzed using microplate readers (EMax, Molecular Devices, Sunnyvale, CA, USA) by collecting optical density values related to living cell concentrations.

## 2.3. Osteoblast Cell Culture and Characterization

SaOS-2 human osteosarcoma cells were employed for cell adhesion and osteoconductivity testing. This cell line was widely used in bone cell differentiation, proliferation, and metabolism research.<sup>[42,43]</sup> The SaOS-2 cells, which are capable of rapid bone production, were cultured and incubated in an osteoblast-inducer medium consisting of 4.5 g/L glucose Dulbecco's modified Eagle medium (DMEM) (D-glucose, L-glutamine, phenol red, and sodium pyruvate) supplemented with 10% fetal bovine serum. They were then allowed to proliferate within Petri dishes for 24 h at 37 °C. When a final concentration of  $5 \times 10^5$  cells  $\text{mL}^{-1}$  was achieved, the cultured cells were deposited on the top surface of each of the composite and control samples. Cell seeding took place in osteogenic medium, which consisted of DMEM supplemented with the following nominal amounts: 50  $\mu\text{g mL}^{-1}$  ascorbic acid,  $10 \times 10^{-3}$  M  $\beta$ -glycerol phosphate,  $100 \times 10^{-3}$  M hydrocortisone, and 10% fetal bovine calf serum. All samples were incubated for 7 days at 37 °C. The medium was changed twice during the incubation period. These cell attachment tests were repeated three times ( $n = 3$ ) for each sample. The average of was then plotted to compare differences. The SaOS-2 cells were stained for fluorescence microscopy with Phalloidin (green; F-actin) and Hoechst 33342 (blue; nuclei) for 1 h and washed three times with 1 mL Tris Buffered Saline with Tween 20 (TBST) solution. Cell counts were performed in a fluorescence microscope (BZ-X700; Keyence, Osaka, Japan).

In the osteoconductivity tests, cell seeding also took place in an osteogenic medium which consisted of DMEM supplemented with about 50  $\mu\text{g mL}^{-1}$  ascorbic acid, about  $10 \times 10^{-3}$  M  $\beta$ -glycerol phosphate,  $100 \times 10^{-3}$  M hydrocortisone, and about 10% fetal bovine calf serum. The test samples were incubated in this medium for 7 days at 37 °C. Results were assessed using a laser microscope and 3D image analyses (VK-X200K series, Keyence, Osaka, Japan). All experiments were repeated in triplicate ( $n = 3$ ). The surfaces were also observed by a field-emission scanning electron microscope (FEG-SEM; Hitachi S-4300SE, Tokyo, Japan).

The formation of bony apatite was also monitored by means of photometric optical density analyses of Alizarin red stain (Alizarin Red S; Sigma-Aldrich) upon staining at 7 days ( $n = 3$ ). Cells were fixed with 4% paraformaldehyde prior to staining. The Alizarin Red stain was removed by washing twice in 95% ethanol for 10 min at room temperature, and 100  $\mu\text{L}$  samples of the dye solution were transferred to 96-well plates. Quantification of staining density was obtained by measuring its concentration in terms of optical absorbance at 405 nm on a plate reader (EMax, Molecular Devices, CA, USA).

The formation of bony apatite was also monitored by means of photometric optical density analyses of Alizarin red stain (Alizarin Red S; Sigma-Aldrich) upon staining at 7 days ( $n = 3$ ). Cells were fixed with 4% paraformaldehyde prior to staining. The Alizarin Red stain was removed by washing twice in 95% ethanol for 10 min at room temperature, and 100  $\mu\text{L}$  samples of the dye solution were transferred to 96-well plates. Quantification of staining density was obtained by measuring its concentration in terms of optical absorbance at 405 nm on a plate reader (EMax, Molecular Devices, CA, USA).

## 2.4. Fourier Transform IR

Time-lapse Fourier transform IR (FTIR) spectra were collected after the osteoconductive tests. FTIR spectra were obtained using a high sensitivity spectroscope (Spectrum100FT-IR/Spotlight400; PerkinElmer Inc., Waltham, MA, USA). The spectral resolution of this equipment was  $0.4\text{ cm}^{-1}$ . Average FTIR spectra targeting the SaOS-2 cell-grown hydroxyapatite were computed for each substrate from five independent measurements performed on  $n = 4$  samples. Pre-processing of raw data included baseline subtraction, smoothing, normalization, and fitting of the raw spectra using commercially available software (Origin 8.5, OriginLab Co., Northampton, MA, USA).

## 2.5. Statistical Analysis

All data were expressed as mean values  $\pm$  one standard deviation and analyzed for their statistical significance ( $p \leq 0.05$ ) according to the unpaired Student's t-test.

## 3. Results

### 3.1. Antibacterial Test Results

Figure 2 summarizes the results of antibacterial tests. In Figure 2a,b, the concentration of living bacteria is shown by two different methods: i) direct counting on CFDA green-stained cells and ii) measurements of the optical density of formazan dye which is proportional to the number of living microorganisms (in the red wavelength interval), respectively. The four sets of images in Figure 2c–f show laser microscopic images of the bacteria-exposed surface (top), DAPI blue fluorescence images of bacterial cell nuclei (middle), and CFDA green fluorescence images of living bacteria (bottom) for monolithic PEEK, PEEK/ $\beta$ -Si $_3$ N $_4$ , PEEK/ $\alpha$ -Si $_3$ N $_4$ , and PEEK/ $\beta$ -SiYAlON, respectively.

Assessments by both direct bacterial cell counting and optical density methods consistently showed that the PEEK/ $\beta$ -Si $_3$ N $_4$  composites had the lowest concentration of living bacteria after 24 h (i.e., exactly one order of magnitude less than that of monolithic PEEK according to the direct counting

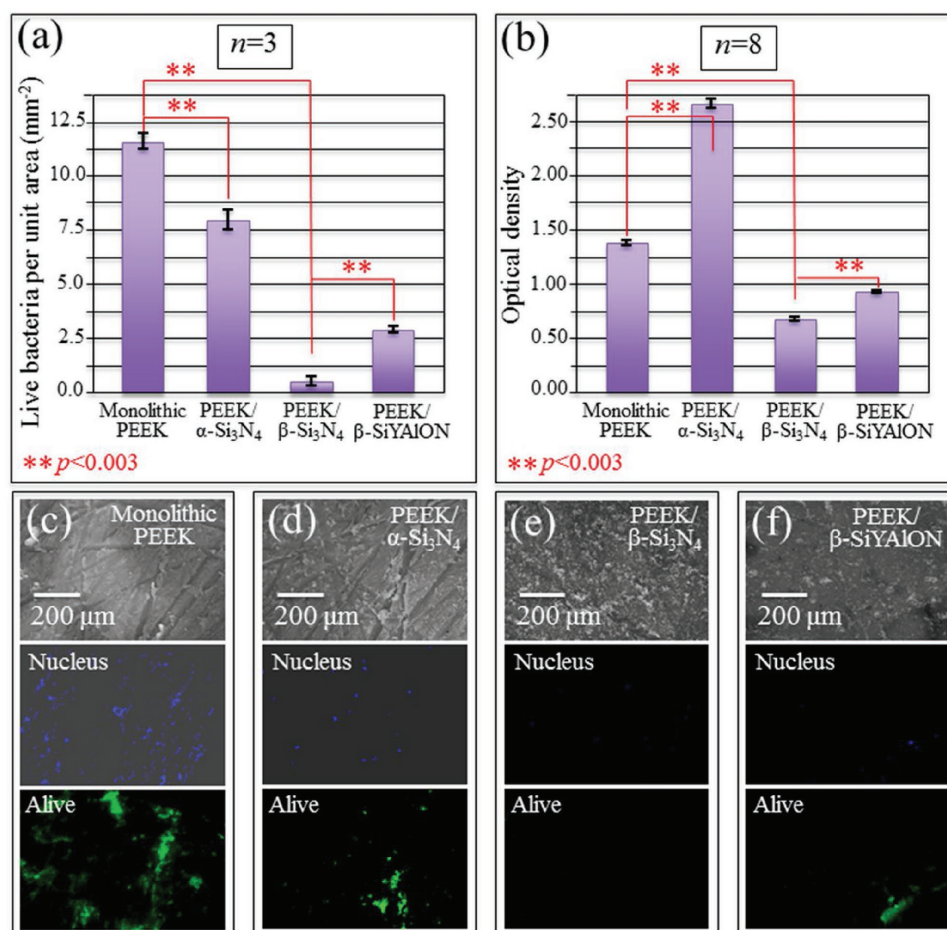


**Figure 2.** Results of antibacterial tests on monolithic PEEK and PEEK-matrix composites: a) counting of living bacteria on CFDA green-stained microscopic images and b) measurements of the optical density of formazan dye. Laser microscopic images of bacteria-exposed surface (top), DAPI blue fluorescence images of bacterial cell nuclei (middle), and CFDA green fluorescence images of living bacteria in c) monolithic PEEK, d) PEEK/ $\beta$ -Si $_3$ N $_4$ , e) PEEK/ $\alpha$ -Si $_3$ N $_4$ , and f) PEEK/ $\beta$ -SiYAlON.

method). Again, according to direct bacterial counting, a significant improvement in bacterial killing capacity of the composite substrate was also detected for the PEEK/ $\beta$ -SiYAlON composite (i.e., more than a fourfold reduction), while the PEEK/ $\alpha$ -Si<sub>3</sub>N<sub>4</sub> composite only experienced an improvement of 30% when compared to monolithic PEEK (cf. Figure 2a). Note that these standard methods for antibacterial evaluation were only qualitatively consistent with each other. The optical density method was biased by strong fluorescence emitted in red frequencies by the PEEK matrix which influenced the results (cf. Figure 2b). Moreover, the  $\alpha$ -Si<sub>3</sub>N<sub>4</sub> powder (a commercially available ceramic raw powder) contained a binder which made it fluorescent in the red interval as well. This circumstance biased the measurements. It was confirmed with a high number of repetitions,  $n = 8$ ). Consequently, the PEEK/ $\alpha$ -Si<sub>3</sub>N<sub>4</sub> composite was the least antibacterial substrate according to the optical density method, which contrasted with the direct counting method (cf. Figure 2a,b). Despite this discrepancy, the overall results of antibacterial testing clearly showed that the addition of a minor fraction of  $\beta$ -Si<sub>3</sub>N<sub>4</sub> or  $\beta$ -SiYAlON particles significantly contributed to an increase in the antibacterial effectiveness PEEK.

### 3.2. Osteoconductivity Test Results

Figure 3a provides a summary of the SaOS-2 cell proliferation tests based on direct cell nuclei counting of the fluorescence-stained microscopic images. Figure 3b–e shows details of the osteoconductivity tests in three sets of microscopic images: i) laser microscopy images of the SaOS-2-cell-exposed surface (top), ii) Hoechst 33342 blue fluorescence images of cell nuclei (middle), and iii) merging microscopic/fluorescence images of living cells (bottom). Figure 3f summarizes the results of the osteoconductivity tests conducted for 7 days as assessed by standardized Alizarin red stain photometric testing of optical density (cf. also photographs of stained samples in Figure S1 of the Supporting Information). These tests, which quantify the process of deposition by cells of bony apatite on different samples, showed that the osteogenic activity of SaOS-2 cells was much improved as compared to that of monolithic PEEK when a fraction of ceramic (either  $\alpha$ -Si<sub>3</sub>N<sub>4</sub> or  $\beta$ -Si<sub>3</sub>N<sub>4</sub> or  $\beta$ -SiYAlON) dispersoids was added to the PEEK matrix. Moreover, such an improvement in hydroxyapatite formation appeared to be substantiated by a statistically meaningful repeatability. Upon comparing Figure 3a,f, it appears that the most efficient particulate

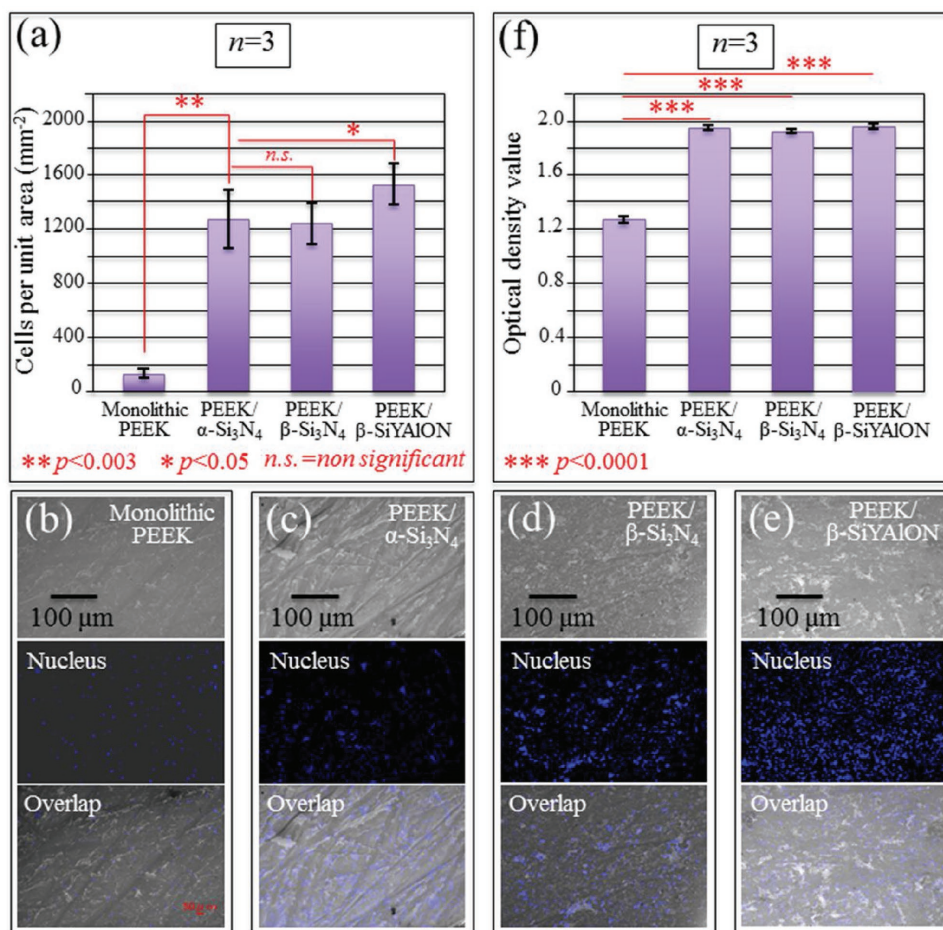


**Figure 3.** a) Results of SaOS-2 cell proliferation test based on direct cell nuclei counting of fluorescence-stained microscopic images. Laser microscopic images of the SaOS-2-cell-exposed surface (top), Hoechst 33342 blue fluorescence images of cell nuclei (middle), and merging microscopic/fluorescence images of living cells (bottom) on b) monolithic PEEK, c) PEEK/ $\beta$ -Si<sub>3</sub>N<sub>4</sub>, d) PEEK/ $\alpha$ -Si<sub>3</sub>N<sub>4</sub>, and e) PEEK/ $\beta$ -SiYAlON substrates. In panel (f), results (with statistics) of photometric optical density experiments upon Alizarin red stain conducted on the same samples mentioned above.

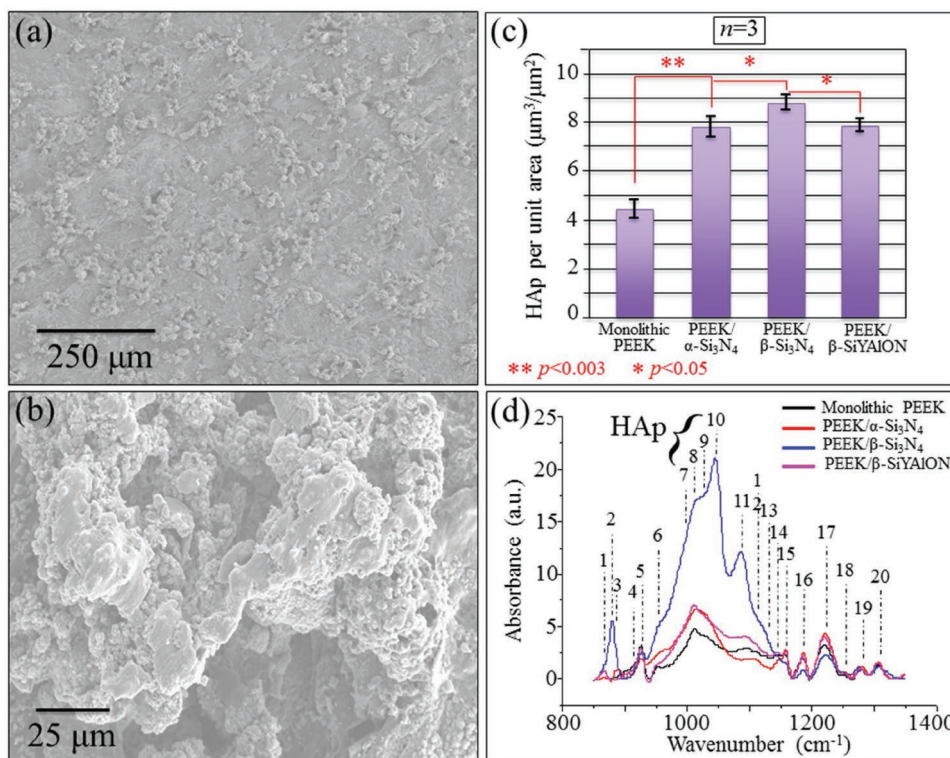


**Figure 4.** a) Low-magnification and b) high-magnification FEG-SEM images of SaOS-2 cell-grown bony apatite on the PEEK/ $\beta$ -Si<sub>3</sub>N<sub>4</sub> substrate; c) the amounts (with statistics) of bony apatite on different substrates after 7 days exposure to SaOS-2 cells as assessed by 3D image analysis-assisted laser microscopy; and d) FTIR spectra of bony apatite grown on different substrates with numbering of sub-band components (cf. Table 1).

dispersion for cell proliferation was  $\beta$ -SiAlON, while all the three investigated composites performed in a quite similar way in terms of bone formation as far as optical density measurements were involved. Note also that the improvement in cell proliferation was as remarkable as 700% in the PEEK/ $\beta$ -Si<sub>3</sub>N<sub>4</sub> composite as compared to monolithic PEEK. In order to better quantify osteogenesis and to clarify the reason for the observed improvement, FEG-SEM observation, 3D image analysis-assisted laser microscopy, and FTIR experiments were conducted after osteoconductivity tests. **Figure 4a,b** shows low- and high-magnification FEG-SEM images of SaOS-2 cell-grown apatite on the PEEK/ $\beta$ -Si<sub>3</sub>N<sub>4</sub> composite substrate after 7 days exposure to osteogenic medium. In **Figure 4c**, a plot is given, which represents the average volume of bony apatite per unit area computed by 3D image analysis on laser microscopic images collected on different composite substrates in comparison with monolithic PEEK substrate tested under the same conditions. Also in this case, data were collected after 7 days exposure in osteogenic medium. The volumetric increases in bony apatite measured by different methods on composites as compared to the monolithic PEEK substrate were also remarkably high:  $\approx 60\%$  and  $\approx 100\%$  for optical density and 3D laser microscopy, respectively. In panel (d) of **Figure 4**, the FTIR spectra of bony apatite on each substrate are deconvoluted into 20 sub-bands. **Table 1** summarizes all of the sub-bands components including the frequency of their maxima and their physical origins.<sup>[44–49]</sup> The prominent features in the FTIR spectra associated with HAp are located in the frequency interval 950–1150 cm<sup>-1</sup>.

**Table 1.** FTIR sub-band components detected in the spectra of **Figure 4b** with the frequency of their maxima and their physical origins.<sup>[44–49]</sup>

Band	Frequency [cm <sup>-1</sup> ]	Assignment
1	865	PEEK
2	878	CO <sub>3</sub> <sup>2-</sup> (B-type)
3	887	SiO <sub>4</sub> <sup>4-</sup> ( $\nu_1$ - HAp)
4	917	Phosphodiester
5	928	PEEK
6	954	PO <sub>4</sub> <sup>3-</sup> ( $\nu_1$ - HAp)
7	995	PO <sub>4</sub> <sup>3-</sup> ( $\nu_1$ - HAp)
8	1014	PO <sub>4</sub> <sup>3-</sup> ( $\nu_1$ - HAp)
9	1030	PO <sub>4</sub> <sup>3-</sup> ( $\nu_3$ - HAp)
10	1045	PO <sub>4</sub> <sup>3-</sup> ( $\nu_3$ - HAp)
11	1076	PO <sub>4</sub> <sup>3-</sup> + CO <sub>3</sub> <sup>2-</sup>
12	1112	PO <sub>4</sub> <sup>3-</sup> (amorphous HAp)
13	1125	PO <sub>4</sub> <sup>3-</sup> ( $\nu_3$ - HAp)
14	1145	HPO <sub>4</sub> <sup>2-</sup>
15	1150	HPO <sub>4</sub> <sup>2-</sup>
16	1163	PO <sub>4</sub> <sup>3-</sup> ( $\nu_3$ - HAp)
17	1239	Amide III (random coil)
18	1250	Amide III ( $\beta$ -sheet)
19	1272	Amide III ( $\alpha$ -helix)
20	1340	CH <sub>2</sub> wagging

Spectroscopic assessments showed the highest FTIR intensities for bony apatite grown on the PEEK/ $\beta$ -Si<sub>3</sub>N<sub>4</sub> composite (cf. Figure 4d). Such an enhanced infrared absorption from the apatite phase might be related to a higher crystallinity of the phase grown on this specific composite substrate.

### 3.3. Other Characterizations

The three types of polymer-matrix composites investigated in this study all contained the same amount of ceramic particles. The Young's moduli of all the composites were between 23 and 27 GPa according to a compressive measurement method,<sup>[50]</sup> while the monolithic PEEK control had a Young's modulus of  $7.5 \pm 0.8$  GPa in good agreement with a prior report.<sup>[10]</sup> All of these stiffness values are comparable to the normal elastic modulus range found in cortical bone.<sup>[51,52]</sup> The composites therefore preserve one of PEEK's important properties that purportedly minimizes subsidence, stress shielding, and bone resorption.<sup>[53]</sup> However, it should also be noted for some devices (e.g., intervertebral spinal spacers), implant design is more important than material composition or Young's modulus in eliminating subsidence and stress shielding.<sup>[54]</sup>

These newly fabricated PEEK-composites were also characterized for their X-ray translucency. **Figure 5** shows an X-ray radiographic images comparing the translucency of the three PEEK composites of this study to monolithic PEEK, monolithic  $\beta$ -Si<sub>3</sub>N<sub>4</sub>, and porous and dense titanium-alloys. Remarkably, the visibility of the PEEK/ $\beta$ -Si<sub>3</sub>N<sub>4</sub> composite was significantly improved as compared to the almost completely transparent monolithic PEEK and it was comparable to monolithic  $\beta$ -Si<sub>3</sub>N<sub>4</sub>. On the other hand, the PEEK/ $\beta$ -SiYAlON composite sample was as visible as the porous and dense titanium samples. The higher detectability of the PEEK/ $\beta$ -SiYAlON sample as compared to the PEEK/ $\beta$ -Si<sub>3</sub>N<sub>4</sub> arises from the relatively high fraction of yttrium in the former sample. X-rays absorbance is determined by the constituent elements of the composites and it has a cubic relationship to atomic number. Consequently, heavier yttrium was

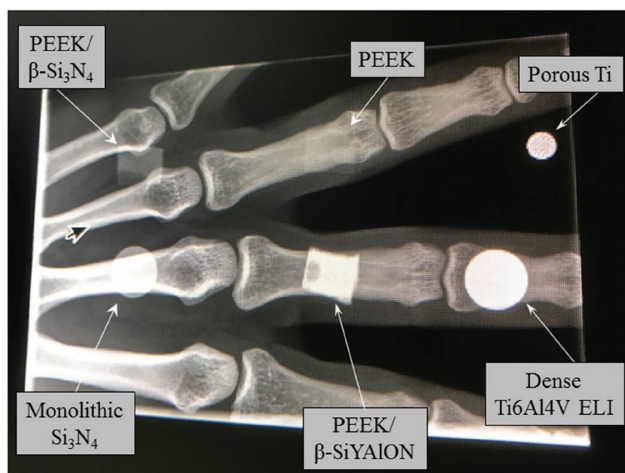


**Figure 5.** X-ray radiograph comparing the translucency performance of the three composites in comparison with the monolithic PEEK control and other biomaterials employed as orthopedic implants.

efficient in increasing the contrast of the PEEK/ $\beta$ -SiYAlON sample. Note that a minor fraction of Y<sub>2</sub>O<sub>3</sub> was also present in the PEEK/ $\beta$ -Si<sub>3</sub>N<sub>4</sub> sample as a sintering aid. X-ray imaging plays an important role in the postoperative evaluation of patients undergoing, for example, spinal surgery. It is believed that the improved compatibility shown in this study for PEEK/ceramic composites will improve clinical imaging and may represent a driving force in promoting their adoption for spinal applications.

## 4. Discussion

The detailed chemical and spectroscopy analyses of a retrieved Si<sub>3</sub>N<sub>4</sub> spinal implant were recently published.<sup>[41]</sup> It showed that elemental silicon and nitrogen were deposited into the crystal lattice of native hydroxyapatite by action of the osteoblasts. The presence of Si and N stimulated progenitor cell differentiation and osteoblastic activity in vivo, which ultimately accelerated bone ingrowth. FTIR analyses and several other spectroscopic techniques confirmed their release from the surface of the Si<sub>3</sub>N<sub>4</sub> implant and their subsequent incorporation into the mineralized apatite structure. An identical analysis was conducted on a retrieved monolithic PEEK spinal implant. There were obviously no chemical changes in the bony apatite surrounding this device and it apparently had lower osteoconductive activity. This prior study confirmed that silicon and nitrogen were key constituents for the upregulation of osseous activity. The crystallographic imperfections introduced by their substitution into native hydroxyapatite apparently led to the enhanced bioactivity of the Si<sub>3</sub>N<sub>4</sub> device. It was this discovery that stimulated the idea of hybridization of PEEK with Si<sub>3</sub>N<sub>4</sub> particles in order to translate this Si/N chemistry to this widely used polymeric material. This was the object of this study. Its effectiveness was confirmed by FTIR spectroscopic fingerprints of silicate tetrahedra within the bony apatite grown by the SaOS-2 cells on the PEEK/ $\beta$ -Si<sub>3</sub>N<sub>4</sub> substrates. **Figure 6a** shows that this composite substrate indeed grew Si-apatite. The vibrational absorbances for (SiO<sub>4</sub>)<sup>4-</sup> and Si—O—Si bonds (cf. labels in inset) were only detected for the PEEK/ $\beta$ -Si<sub>3</sub>N<sub>4</sub> substrate and not for monolithic PEEK (cf. lower and upper spectra, respectively).

Similar in situ FTIR experiments were conducted on living bacteria in a search for spectroscopic fingerprints of their metabolism on PEEK/ $\beta$ -Si<sub>3</sub>N<sub>4</sub> and monolithic PEEK substrates. The FTIR spectra of **Figure 6b** displayed markedly different features for these two substrates (cf. upper and lower spectrum for bacteria on PEEK/ $\beta$ -Si<sub>3</sub>N<sub>4</sub> and monolithic PEEK substrates, respectively). Note that the spectrum of *S. epidermidis* in the interval 2800–3000 cm<sup>-1</sup> mainly represents C—H bond vibrations.<sup>[55]</sup> Significant reductions in CH<sub>2</sub> and CH<sub>3</sub> vibrational intensities for bacterial membrane lipids and proteins were detected when *S. epidermidis* was exposed to the PEEK/ $\beta$ -Si<sub>3</sub>N<sub>4</sub> substrates. No apparent changes were observed for the bacterial exposed to monolithic PEEK (cf. labels in inset to **Figure 6b**). This difference was interpreted as degradation of the bacterial membrane, which ultimately led to its disruption and to bacterial lysis.<sup>[56]</sup> It is known that the emission of ammonia, which ultimately leads to the enhancement of extracellular pH and to the formation of free radicals, is lethal to several types of bacteria.<sup>[38,57]</sup>

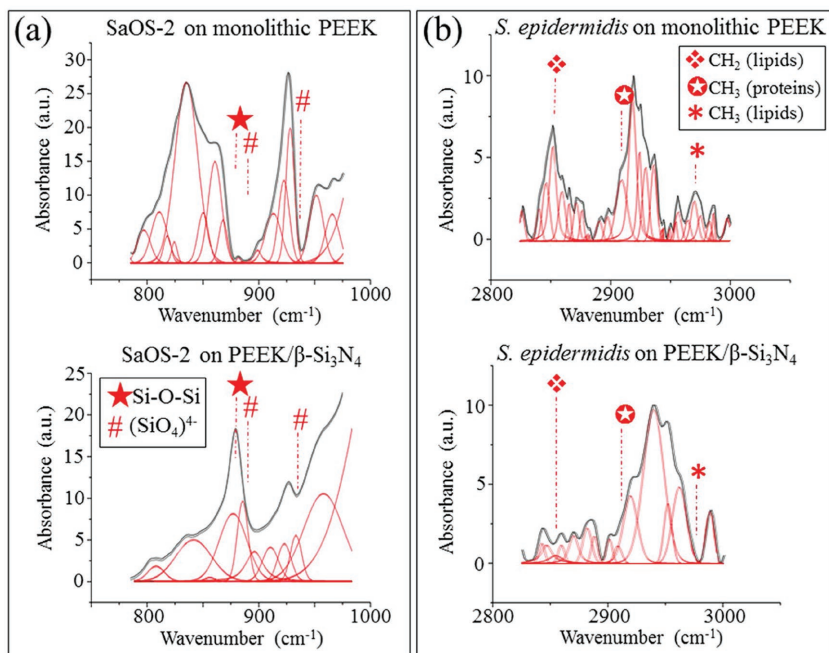
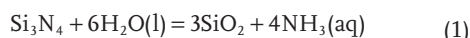


**Figure 6.** a) Spectral deconvolution on FTIR spectra collected in situ on living *S. epidermidis* exposed for 24 h to monolithic PEEK (upper) and PEEK/β-Si<sub>3</sub>N<sub>4</sub> (lower) substrates. The chemical fingerprints of bacterial lysis are emphasized by labels in the inset. b) Spectral deconvolution on FTIR spectra collected in situ on the bony apatite deposited by living SaOS-2 cell (7 days exposure) on monolithic PEEK (upper) and PEEK/β-Si<sub>3</sub>N<sub>4</sub> (lower) substrates. The fingerprints of chemical species characteristics of Si-apatite are emphasized with labels in the inset.

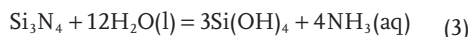
Based on data from prior literature along with the results from the current study, shown in Figure 7a,b are proposed molecular models summarizing the interactions between the PEEK/β-Si<sub>3</sub>N<sub>4</sub> composite and *S. epidermidis*. These models provide an enlarged view of the chemical interactions between the bacteria's membrane and the biological environment in the neighborhood of the Si<sub>3</sub>N<sub>4</sub> particles. Elution of ammonia from these particles is believed to be the chemical trigger which results in a cascade of reactions that ultimately leads to *S. epidermidis* lysis. Note that this study has only confirmed antibacterial effect versus a gram-positive bacterium, while the effectiveness versus gram-negative bacteria remains yet to be confirmed for the PEEK/β-Si<sub>3</sub>N<sub>4</sub> composite. However, ammonia elution has proved effective also versus gram-negative bacteria in experiments on bulk β-Si<sub>3</sub>N<sub>4</sub>.<sup>[13]</sup>

Similarly, the interaction between PEEK/β-Si<sub>3</sub>N<sub>4</sub> and SaOS-2 cells, which includes the elution of orthosilicate molecules from the Si<sub>3</sub>N<sub>4</sub> ceramic particles, is provided in Figure 7c; while in Figure 7d is an enlarged view of the chemical interaction between the cell membrane and the

Elution of ammonia is a well-known phenomenon in β-Si<sub>3</sub>N<sub>4</sub> exposed to aqueous solution<sup>[58,59]</sup> and a pH buffering effect has been documented as well for this material.<sup>[38]</sup> In aqueous environment, two surface reactions concurrently occur, as follows<sup>[59]</sup>



The overall reaction could then be expressed as follows



The Gibbs energy of the above reaction in Equation (3) has been reported as a negative value of  $-1268.72 \text{ kJ mol}^{-1}$  (with a quite high equilibrium constant at room temperature equal to  $1.57 \times 10^{96}$ ), which explains the spontaneous elution of both ammonia and silicic acid from the Si<sub>3</sub>N<sub>4</sub> surface.

In substance, the current FTIR results support the data shown in Figure 2 and suggest that the antibacterial effect previously reported for bulk Si<sub>3</sub>N<sub>4</sub><sup>[13]</sup> can be translated to PEEK by the addition of a dispersion of Si<sub>3</sub>N<sub>4</sub> particles.

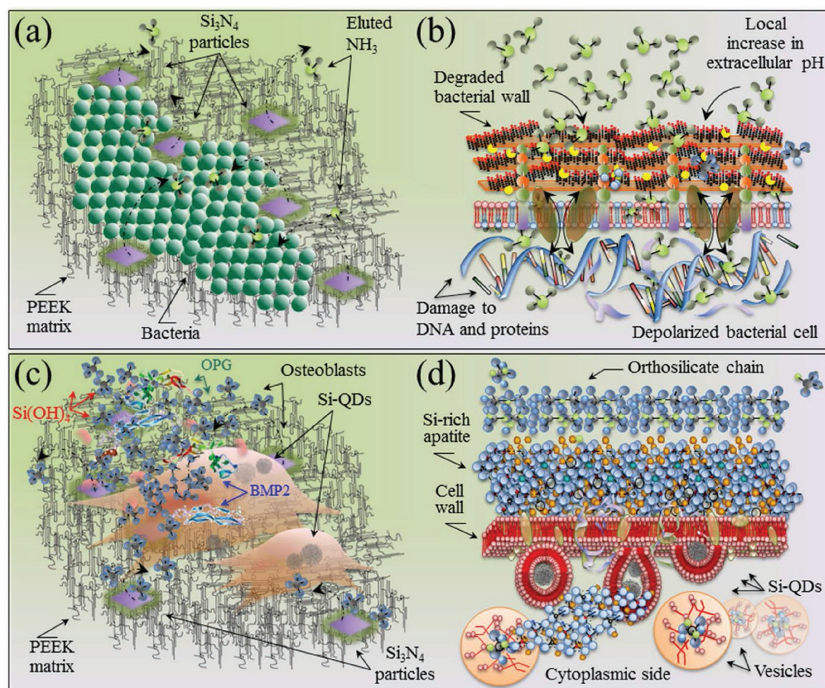


**Figure 7.** a) Interaction between PEEK/β-Si<sub>3</sub>N<sub>4</sub> and *S. epidermidis* with the elution of ammonia from the ceramic particles and b) an enlarged view of the chemical interaction between the bacteria membrane and the biological environment in the neighborhood of the Si<sub>3</sub>N<sub>4</sub> particles. In panel (c), interactions between PEEK/β-Si<sub>3</sub>N<sub>4</sub> and SaOS-2 cells with the elution of orthosilicate from the ceramic particles and d) an enlarged view of the chemical interaction between the cell membrane and the biological environment in the neighborhood of the Si<sub>3</sub>N<sub>4</sub> particles.

biological environment in the vicinity of the  $\text{Si}_3\text{N}_4$  particles. This last figure also envisages the formation of endocytotic vesicles around orthosilicate clusters<sup>[60]</sup> and silicon quantum dots (Si-QDs) which were detected in SaOS-2 cell grown bony tissue reported in a previous study.<sup>[61]</sup>

## 5. Limitations of This Study

The main limitation of this study consists of the fact that the improvements with respect to monolithic PEEK could so far only be proved in vitro. The possibility that the composite will also show the same improvements in both osteoconductivity and bacteriostasis when implanted in the human body remains yet to be demonstrated. Moreover, future in vitro testing using mesenchymal progenitor cells and gram-negative bacterial strains could serve to demonstrate eventual osteoinductive properties and to further validate the range of antibacterial efficiency of the proposed composites.

Regarding the use of the composites in vivo, elution of ceramic particles could in principle occur upon friction or during implantation surgery. However, this has not been considered here to be a concern because of the following three reasons: i) the microscopic interface bonding between ceramic particles and PEEK matrix appeared quite strong and coherent, with no detachment of silicon nitride particles being observed during machining or polishing; ii) the ceramic particles have a size in the order of several micrometers and thus their size does not fall in the reactive and potentially toxic nanometer scale; iii) silicon nitride is a perfectly biocompatible (and osteogenic) material as demonstrated by the bulk silicon nitride spinal implants used around the world since the last  $\approx 10$  years. In spinal implants made of the newly proposed composite, the risk of particle elution is thus not higher than the risk related to micrometric debris detachment from the roughened surface of titanium or PEEK or even bulk silicon nitride composites.

## 6. Conclusion

This study demonstrated that hybridization of PEEK by incorporating a dispersion of  $\text{Si}_3\text{N}_4$  particles via melt blending was an effective approach to improving both the polymer's lack of bioactivity and its proneness to bacterial proliferation. The resulting composites preserved the positive characteristics of monolithic PEEK (i.e., elastic modulus equivalent to cortical bone) while improving its X-ray imaging compatibility. More importantly, the PEEK/ $\beta\text{-Si}_3\text{N}_4$  composite demonstrated one order-of-magnitude reduction in live *S. epidermidis* as compared to monolithic PEEK. This result is particularly relevant in the prevention of periprosthetic infections and early implant failures, as this bacterium is most frequently reported as the main responsible for early implant replacements.<sup>[62]</sup> Hybridization of PEEK with  $\beta\text{-Si}_3\text{N}_4$  particles also demonstrated remarkable in vitro improvements of 700% and 100% in SaOS-2 cell proliferation and bone formation, respectively, when compared to monolithic PEEK. In conclusion, while more detailed in vitro and in vivo studies need to be performed to confirm the viability of PEEK/ $\text{Si}_3\text{N}_4$  composites, this simple fabrication

method which exploits Si/N chemistry could beneficially replace monolithic PEEK implants for various trauma, prosthodontics, maxillofacial, and cranial procedures.

## Supporting Information

Supporting Information is available from the Wiley Online Library or from the author.

## Acknowledgements

The authors thank Mr. S. Horiguchi for his kind help during the experimental procedures with SaOS-2 and *S. epidermidis* experiments.

## Conflict of Interest

Prof. Pezzotti is a scientific consultant of Amedica Corp. Dr. Bal, Dr. McEntire and Dr. Bock work for Amedica Corp. Mr. Kitajima and Mr. Inada work for Otsuka Chemical Corp.

## Keywords

antibacterial, composite, osteoconductive, polyetheretherketone, silicon nitride

Received: January 23, 2018

Revised: March 15, 2018

Published online:

- [1] D. Williams, *Med. Device Technol.* **2008**, 19, 10.
- [2] L. Eschbach, *Injury* **2000**, 31, 22.
- [3] T. U. Jiya, T. Smit, B. J. Van Royen, M. Mullender, *Eur. Spine J.* **2011**, 20, 618.
- [4] Z. P. Lu, K. Friedrich, *Wear* **1995**, 181.
- [5] A. Godara, D. Raabe, S. Green, *Acta Biomater.* **2007**, 3, 209.
- [6] L. M. Wenz, K. Merritt, S. A. Brown, A. Moet, A. D. Steffe, *J. Biomed. Mater. Res.* **1990**, 24, 207.
- [7] C. H. Rivard, S. Rhalmi, C. Coillard, *J. Biomed. Mater. Res.* **2002**, 62, 488.
- [8] T. Nieminen, I. Kallela, E. Wuolijoki, H. Kainulainen, I. Hiidenheimo, I. Rantala, *J. Biomed. Mater. Res., Part A* **2008**, 84A, 377.
- [9] A. Katzer, H. Marquardt, J. Westendorf, J. V. Wening, G. von Foerster, *Biomaterials* **2002**, 23, 1749.
- [10] H. Wang, M. Xu, W. Zhang, D. T. Kwok, J. Jiang, Z. Wu, P. K. Chu, *Biomaterials* **2010**, 31, 8181.
- [11] J. M. Toth, M. Wang, B. T. Estes, J. L. Scifert, H. B. Seim, A. S. Turner, *Biomaterials* **2006**, 27, 324.
- [12] R. H. Khonsari, P. Berthier, T. Rouillon, J.-P. Perrin, P. Corre, *J. Oral Maxillofac. Surg., Med. Pathol.* **2014**, 26, 477.
- [13] R. M. Bock, E. N. Jones, D. A. Ray, B. S. Bal, G. Pezzotti, B. J. McEntire, *J. Biomed. Mater. Res., Part A* **2017**, 105, 1521.
- [14] T. J. Webster, A. A. Patel, M. N. Rahaman, B. S. Bal, *Acta Biomater.* **2012**, 8, 4447.
- [15] D. J. Gorth, S. Puckett, B. Ercan, T. J. Webster, M. Rahaman, B. S. Bal, *Int. J. Nanomed.* **2012**, 7, 4829.
- [16] A. J. Barton, R. D. Sagers, W. G. Pitt, *J. Biomed. Mater. Res.* **1996**, 30, 403.
- [17] S. M. Kurtz, J. N. Devine, *Biomaterials* **2007**, 28, 4845.



- [18] I. V. Panayotov, V. Orti, F. Cuisinier, J. Yachouh, *J. Mater. Sci.: Mater. Med.* **2016**, *27*, 118.
- [19] M. R. Abdullah, A. Goharian, M. R. Abdul Kadir, M. U. Wahit, *J. Biomed. Mater. Res., Part A* **2015**, *103*, 3689.
- [20] B. D. Ratner, A. S. Hoffman, *Physicochemical Surface Modification of Materials Used in Medicine BT, – Biomaterials Science*, 3rd ed. (Eds: B. D. Ratner, A. S. Hoffman, F. J. Schoen, J. E. Lemons), Academic Press, Waltham, MA, USA **2013**, pp. 259–276.
- [21] R. Ma, T. Tang, *Int. J. Mol. Sci.* **2014**, *15*, 5426.
- [22] E. T. J. Rochford, D. J. Jaekel, N. J. Hickok, R. G. Richards, T. F. Moriarty, A. H. C. Poulsson, *Bacterial Interactions with Polyaryletheretherketone* (Ed: S. M. Kurtz), Elsevier Academic Press, New York, NY, USA **2012**, pp. 93–117.
- [23] R. C. Spencer, *J. Hosp. Infect.* **1999**, *43*, S127.
- [24] M. P. Pai, S. L. Pendland, L. H. Danziger, *Ann. Pharmacother.* **2001**, *35*, 1255.
- [25] J. M. Schierholz, N. Yucel, A. F. Rump, J. Beuth, G. Pulverer, *Int. J. Antimicrob. Agents* **2002**, *19*, 511.
- [26] C. S. Adams, V. Antoci, G. Harrison, P. Patal, T. A. Freeman, I. M. Shapiro, J. Parvizi, N. J. Hickok, S. Radin, P. Ducheyne, *J. Orthop. Res.* **2009**, *27*, 701.
- [27] L. A. Mermel, *Emerg. Infect. Dis.* **2001**, *7*, 197.
- [28] D. J. Kilgus, D. J. Howe, A. Strang, *Clin. Orthop. Relat. Res.* **2002**, *404*, 116.
- [29] C. Canal, R. Molina, E. Bertran, P. Erra, *J. Adhes. Sci. Technol.* **2004**, *18*, 1077.
- [30] K. H. Tan, C. K. Chua, K. F. Leong, C. M. Cheah, P. Cheang, M. S. Abu Bakar, S. W. Cha, *Biomaterials* **2003**, *24*, 3115.
- [31] F. Furno, K. S. Morley, B. Wong, B. L. Sharp, P. L. Arnold, S. M. Howdle, R. Bayston, P. D. Brow, P. D. Winship, H. J. Reid, *J. Antimicrob. Chemother.* **2004**, *54*, 1019.
- [32] Y. Zhang, L. Hao, M. M. Savalani, R. A. Harris, L. Di Silvio, K. E. Tanner, *J. Biomed. Mater. Res., Part A* **2009**, *91A*, 1018.
- [33] J. P. Ruparelia, A. Kumar, S. P. Duttgupta, *Acta Biomater.* **2008**, *4*, 707.
- [34] R. P. Allaker, *J. Dent. Res.* **2010**, *89*, 1175.
- [35] W. K. Jung, H. C. Koo, K. W. Kim, S. Shin, S. H. Kim, Y. H. Park, *Appl. Environ. Microbiol.* **2008**, *74*, 2171.
- [36] U. Samuel, J. P. Guggenbichler, *Int. J. Antimicrob. Agents* **2004**, *23*, 75.
- [37] G. Perrelli, G. Piolatto, *Sci. Total Environ.* **1992**, *120*, 93.
- [38] G. Pezzotti, R. M. Bock, B. J. McEntire, E. Jones, M. Boffelli, W. Zhu, G. Baggio, F. Boschetto, L. Puppulin, T. Adachi, T. Yamamoto, N. Kanamura, Y. Marunaka, B. S. Bal, *Langmuir* **2016**, *32*, 3024.
- [39] G. Pezzotti, B. J. McEntire, R. M. Bock, W. Zhu, F. Boschetto, A. Rondinella, F. Boschetto, B. McEntire, K. Yamamoto, B. S. Bal, *ACS Biomater. Sci. Eng.* **2016**, *2*, 1121.
- [40] G. Pezzotti, R. M. Bock, T. Adachi, A. Rondinella, F. Boschetto, W. Zhu, E. Marin, B. McEntire, B. S. Bal, O. Mazda, *Appl. Mater. Today* **2017**, *9*, 82.
- [41] G. Pezzotti, N. Oba, W. Zhu, E. Marin, A. Rondinella, F. Boschetto, B. McEntire, K. Yamamoto, B. S. Bal, *Acta Biomater.* **2017**, *64*, 411.
- [42] H. C. Anderson, H. H. Hsu, P. Raval, T. R. Hunt, J. R. Schwappach, D. C. Morris, D. J. Schneider, *Clin. Orthop. Relat. Res.* **1995**, *313*, 129.
- [43] T. R. Hunt, J. R. Schwappach, H. C. Anderson, *J. Bone Jt. Surg.* **1996**, *78*, 41.
- [44] C. Rey, M. Shimizu, B. Collins, M. J. Glimcher, *Calcif. Tissue Int.* **1991**, *49*, 383.
- [45] H. Boyar, B. Turan, F. Severcan, *Spectroscopy* **2003**, *17*, 627.
- [46] G. S. Mandair, M. D. Morris, *BoneKEy Rep.* **2015**, *4*, 620.
- [47] R. M. Silverstein, G. C. Bassler, T. C. Morrill, *Spectroscopic Identification of Organic Compounds*, 5th ed., John Wiley & Sons, Ltd., New York, NY, USA **1991**.
- [48] D. Marchat, M. Zymelka, C. Coelho, L. Gremillard, L. Joly-pottuz, F. Babonneau, C. Esnouf, J. Chevalier, D. Bernache-Assollant, *Acta Biomater.* **2013**, *9*, 6992.
- [49] G. Ulian, G. Valdré, M. Corno, P. Ugliengo, *Am. Mineral.* **2013**, *98*, 752.
- [50] Standard Test Method for Compressive Properties of Rigid Plastics, *ASTM* **2017**, D695, <https://www.astm.org/Standards/D695.htm>.
- [51] J. Y. Rho, T. Y. Tsui, G. M. Pharr, *Biomaterials* **1997**, *18*, 1325.
- [52] T. S. Keller, Z. Mao, D. M. Spengler, *J. Orthop. Res.* **1990**, *8*, 592.
- [53] P. J. Rao, M. H. Pelletier, W. R. Walsh, R. J. Mobbs, *Orthop. Surg.* **2014**, *6*, 81.
- [54] P. B. Suh, C. Puttlitz, C. Lewis, S. Bal, K. McGilvray, *J. Am. Acad. Orthop. Surg.* **2016**, 160.
- [55] K. Maquelin, C. Kirschner, L. P. Choo-Smith, N. Van Den Braak, H. P. Endtz, D. Naumann, G. J. Puppels, *J. Microbiol. Methods* **2002**, *51*, 255.
- [56] C. El Amri, C. Lacombe, K. Zimmerman, A. Ladram, M. Amiche, P. Nicolas, F. Bruston, *Biochemistry* **2006**, *45*, 14285.
- [57] F. C. Fang, *J. Clin. Invest.* **1997**, *99*, 2818.
- [58] R. C. Dante, C. K. Kajdas, *Wear* **2012**, *288*, 27.
- [59] F. Zhou, X. Wang, K. Adachi, K. Kato, *Surf. Coat. Technol.* **2008**, *202*, 3519.
- [60] C. Y. Wu, J. Martel, W. Y. Cheng, C. C. He, D. M. Ojcius, J. D. Young, *J. Biol. Chem.* **2013**, *288*, 30571.
- [61] G. Pezzotti, E. Marin, T. Adachi, A. Rondinella, F. Boschetto, W.-L. Zhu, N. Sugano, R. M. Bock, B. McEntire, S. B. Bal, *Sci. Rep.* **2017**, *7*, 44848.
- [62] T. Kitao, *J. Infect. Chemother.* **2003**, *9*, 30.